Process Safety and Environmental Protection 201 (2025) 107475

Contents lists available at ScienceDirect

Process Safety and Environmental Protection

journal homepage: www.journals.elsevier.com/process-safety-and-environmental-protection

Carbonation of digested sewage sludge-based sealing material in a final landfill cover system: Role of waterglass and additional industrial by-products

Xuan Ling [a,b], Yuxuan Chen [c,*], Katrin Schollbach [b], H.J.H. Brouwers [a,b]

[a] State Key Laboratory of Silicate Materials for Architectures, Wuhan University of Technology, Wuhan 430070, PR China
[b] Department of the Built Environment, Eindhoven University of Technology, P.O. Box 513, Eindhoven 5600 MB, the Netherlands
[c] School of Civil Engineering, Wuhan University, Wuhan 430072, PR China

ARTICLE INFO

Keywords:
Carbonation
Sewage sludge
Sealing materials
Permeability
Leaching

ABSTRACT

Landfills emit significant greenhouse gases, particularly methane (CH_4) and carbon dioxide (CO_2), yet the interaction between CO_2 and landfill sealing materials remains underexplored. This study investigated the carbonation behavior of sealing materials composed of digested sewage sludge (DSS), waterglass, aggregates, and various industrial by-products as additives—waste incineration fly ash (WIFA), biomass bottom ash (BBA), and aluminum anodizing waste (AAW). An accelerated carbonation process was employed to simulate CO_2 diffusion, and the effects of waterglass and additives on permeability, physicochemical properties, and environmental impacts of the sealing materials with/without carbonation were systematically evaluated. Results show that waterglass improves impermeability by binding particles and filling pores; however, its high alkalinity initially promotes the dissolution of minerals such as boehmite in AAW, increasing porosity. Among the additives, AAW, with its finer particle size, yielded the lowest permeability in uncarbonated samples. Carbonation led to the formation of carbonates and monohydrocalcite, causing phase volume changes that increased porosity and reduced sealing performance. Despite this, overall permeability remained within the acceptable limit ($< 6.34 \times 10^{-10}$ m/s) specified by Dutch regulations, owing to relatively moderate phase transformations. However, carbonation increased the leaching of elements such as Cl and Sb, particularly in DDS-WIFA samples, indicating that carbonation breaks down particles and diminishes physical encapsulation of these toxic elements. This highlights the need for selecting additives with low leachability for environmental compliance. Moreover, a higher dosage of waterglass (2.0 wt%) mitigated impermeability degradation by forming silicate gels and promoting CO_2 adsorption. These findings advance the understanding of carbonation mechanisms in sludge-based sealing materials and inform the selection of feasible industrial by-products for sustainable landfill cover systems.

1. Introduction

Annually, thousands of tons of municipal solid waste are generated globally, with a massive portion directed to landfills, establishing landfills as still crucial components in worldwide waste management. When the landfills reach the designed waste capacity, their closure necessitates a comprehensive cover system to regulate water infiltration and prevent the emission of landfill gas into the atmosphere post-closure (Egloffstein, 2001). These landfill cover systems typically comprise multiple layers of materials, including the support layer, sealing layer, drainage layer and vegetation layer, each meticulously engineered to serve distinct functions (Rijkswaterstaat Bodem+, 1991).

The sealing layer, a vital component of the system, is designed for extremely low permeability and is generally manufactured using clay or clay-containing materials (Wagner, 2013). In recent years, efforts to conserve natural clay resources and promote waste recycling have led to the exploration of industrial by-products, such as sewage sludge (Liu et al., 2022), fly ash (Herrmann et al., 2009), and steel slag (Herrmann et al., 2010), as alternative materials for landfill sealing layers. Sewage sludge, in particular, has gained significant attention due to its wide availability and potential for recycling (He et al., 2015; Hyun and Kim, 2012; Li et al., 2014; Rosli et al., 2020). In the Netherlands, approximately 1.3 million tons of sewage sludge is produced per year, according to the Dutch Water Authorities, incurring a cost of 115 ~ 250 M€ per

* Corresponding author.
E-mail address: yuxuan.chen@whu.edu.cn (Y. Chen).

https://doi.org/10.1016/j.psep.2025.107475
Received 24 September 2024; Received in revised form 4 May 2025; Accepted 17 June 2025
Available online 18 June 2025

year for disposal and treatment (Grootjes et al., 2019). Utilizing sewage sludge in landfill cover systems presents an opportunity to address waste management challenges while reducing costs and carbon emissions (Taki et al., 2020).

Achieving a sealing layer with reduced permeability is possible through the application of sewage sludge in combination with other industrial by-products (Liu et al., 2022; Rubinos and Spagnoli, 2018). Additives such as lime, crushed concrete, and incineration ash have been utilized to improve the mechanical properties of these materials by forming cementitious products that bind particles together (Ayininuola and Ayodeji, 2016; Iqbal et al., 2019; Lin et al., 2007). Rosli et al. proposed the formation of calcium silicate hydrate gels in landfill-sealing materials prepared with sewage sludge and red gypsum (Rosli et al., 2020), while Li et al. identified calcium silicate hydrate and ettringite as the primary hydration products in a dewatered sludge-fly ash-lime system through microstructure analyses (Li et al., 2014). In previous research, sludge-based sealing materials incorporating by-products from sewage, digestate, and incineration industries were developed, with a focus on their low permeability, mineralogical composition and environmental impacts (Ling et al., 2024a).

However, it must be noted that in addition to rainwater infiltration, significant landfill gas emissions, predominantly methane (CH_4) and carbon dioxide (CO_2) in equal volumetric ratios (50 %v/v) (Sadasivam and Reddy, 2015), can still permeate the landfill cover system, even when a gas collection system is installed to mitigate these emissions (Barlaz et al., 2009; Spokas et al., 2006). In older and abandoned landfills, where implementing a gas collection system is often economically or practically unfeasible, fugitive emissions from landfills have emerged as a significant concern. While conventional clay-based sealing materials may not raise durability concerns post-CO_2 diffusion, as there is limited carbonate-forming potential, alternative landfill sealing materials containing higher levels of calcium from industrial waste materials warrant attention. The presence of calcium-containing minerals, as well as the formed calcium silicate hydrates and ettringite, in these materials poses a considerable risk to their stability, as these minerals are prone to carbonation (Liu et al., 2021; Shi et al., 2018). This carbonation process leads to the formation of calcite and subsequent changes in phase volumes, and increased porosity (Dung et al., 2021), particularly in the capillary pore size range of approximately 100–2000 nm, which also accelerates water diffusion within the matrix (Wang et al., 2020). Unfortunately, to the best of the authors' knowledge, few studies have revealed the effects of CO_2 on the permeability and microstructure of sludge-based sealing materials. This limitation may impede the application and effective durability assessment of sealing materials composed of industrial wastes such as sewage sludge.

In this study, the challenge of enhancing the carbonation resistance of sludge-based sealing materials is addressed by proposing two strategies. 1) Enhancing the impermeability of sludge-based material matrix to slow down the penetration of CO_2. Building on the findings of Gartung et al. (2010), who demonstrated that the addition of waterglass, polymers, or other suitable chemicals can reduce the permeability of mineral sealing materials, the potential effect of waterglass on carbonation resistance was investigated. It is noteworthy that the sodium ions introduced by waterglass act as soluble metal cations, which eliminate the formation of carbonate. However, considering that waterglass may react with CaO to form C-S-H gels, which can be carbonated and increase porosity, an evaluation of different waterglass concentrations to balance these effects was conducted. 2) Controlling the calcium oxide content in the industrial waste materials used. To explore the impact of calcium oxide content on carbonation behavior, three distinct industrial wastes were employed as additives: waste incineration fly ash, biomass bottom ash and aluminum anodizing waste. The first two materials, sourced from the incineration industry, contain close to 30 % CaO, while the aluminum anodizing waste, from the aluminum anodizing industry, is nearly free of CaO. Previous research has shown that the combined use of lime and waterglass can improve the compatibility and water permeability of waste rock from coal mining (Wiśniewska and Stępniewski, 2006), as the pore volume of the barrier system is reduced by the formed precipitations due to the chemical reaction. However, the carbonation behavior of these newly proposed sludge-based sealing materials has not been thoroughly investigated, and the interaction between waterglass and these additives remains not fully understood.

This work aims to deepen the understanding of the carbonation behavior in sludge-based sealing materials by employing an accelerated carbonation process to simulate CO_2 diffusion. The potential effect of waterglass and various additives on the permeability, reaction products, and volume stability were characterized through multiple analyses, including X-ray diffraction (XRD), Thermal Gravimetry test (TG), Fourier-Transform Infrared (FT-IR), nitrogen adsorption. Additionally, the environmental impact of the sealing materials post-carbonation is evaluated through leaching tests. The findings provide a foundation for optimizing the use of waterglass and industrial by-products in sludge-based sealing materials, contributing to the development of more durable and sustainable landfill cover systems.

2. Materials and experiments

2.1. Raw materials

Digested sewage sludge (DSS), sourced from a local Wastewater Treatment Plant in Deventer, The Netherlands, served as the matrix materials in this study. Three distinct industrial by-products with varying characteristics were incorporated as additives in the formulation of sludge-based sealing materials. Biomass bottom ash (BBA) was from a grate furnace, where wooden waste materials underwent incineration. Waste incineration fly ash (WIFA) was obtained from a Dutch municipal solid waste plant, with the fly ash separated using electrostatic precipitators. Aluminum anodizing waste (AAW) was the residues generated during the aluminum anodizing process in the alumina industry. Waterglass (WG) (20.1 % Na_2O and 62.7 % SiO_2, PQ France) was introduced to reduce overall permeability in the sealing material formulation (Boels et al., 2005). A high-modulus waterglass was selected for its ability to promote the formation of denser and more impermeable layers. It has also demonstrated promising impermeability performance in previous studies involving residue-based sealing materials (Ling et al., 2024a). In addition, a blend comprising 30 wt% blasting grit and 70 wt% normal sand was utilized as aggregate.

The chemical composition of the raw materials was analyzed using X-ray fluorescence (XRF) on a PANalytical Epsilon 3 instrument. The borate fusion method was used to prepare fuse beads. The results are

Table 1
Chemical composition and physical properties of raw materials.

Elements	DSS	WIFA	BBA	AAW	WG
Na_2O	0.1	4.7	-	4.2	20.1
MgO	0.9	0.9	1.6	-	-
Al_2O_3	0.7	2.6	2.5	55.2	-
SiO_2	2.6	6.8	20.8	0.8	62.7
P_2O_5	4.5	0.5	1.4	0.2	-
SO_3	1.9	8.9	5.8	11.8	-
K_2O	0.5	8.9	4.8	-	-
CaO	4.9 [2.4]	28.9 [6.3]	34.5 [7.1]	1.0 [0]	-
TiO_2	0.4	2.3	8.5	-	-
Fe_2O_3	18.1	3.1	7.2	0.6	-
ZnO	0.5	3.8	1.7	-	-
Cl	0.1	17.6	1.6	-	-
Others	0.6	2.1	2.3	2.4	-
LOI	64.2	8.8	7.3	23.8	17.2
Specific gravity (cm^3/g)	1.69	2.74	2.87	2.54	2.42
Moisture (%)	66.6	1.0	0.6	76.0	-

[] represents CaO content from the calcite within the raw materials based on their TG results (see supplementary materials Figure S1). M_{CaO} % = (Mass loss between 550 °C and 800 °C) × 56/44 × 100 %.

presented in Table 1. The mineral composition of raw materials was determined through X-ray diffraction (Bruker D4 phaser), as shown in Fig. 1. DSS comprises quartz (PDF# 83–2465), calcite (PDF#72–1937), and baricite (PDF#72–1937). WIFA and BBA contain anhydrite (PDF#72–0916), formed during the incineration for sulfur dioxide control. WIFA exhibits high halite and potassium chloride peaks, which are attributed to the disposal of K- and Na-contained waste materials during incineration. AAW contains low-crystalline boehmite (PDF#49–0133), bayerite (PDF#01–0287), and thenardite (PDF#05–0631). The particle size distribution of raw materials was determined using a laser light scattering technique (Mastersizer 2000, Malvern). Raw materials were dispersed in isopropanol with a 10 min ultrasonic dispersion to prevent agglomeration, and the results are depicted in Fig. 2. The average particle size (d50) for DSS, WIFA, BBA, and AAW are approximately 18 μm, 57 μm, 138 μm, and 11 μm, respectively.

2.2. Specimen preparation

As detailed in Table 2, the formulated mixtures consist of a 45 wt% sand fraction, 46 wt% DSS, and 9 wt% additives. Additional 1.5 wt% and 2.0 wt% WG were incorporated based on previous literature recommendations for its application in sealing materials, falling within the range of 1–5 wt% (Boels et al., 2005). It is important to note that, in order to reduce the material costs and enhance the economic feasibility of the mix design, a higher dosage of waterglass was avoided. To ensure the homogeneity of samples mixing, a two-step mixing procedure was adopted. First, the matrix materials (sludge and grain fraction) were blended using a laboratory mixer at a medium speed for approximately 3 min to achieve a uniform base. Subsequently, the additives and WG were gradually added during continued mixing for an additional 3 min, ensuring their uniform dispersion throughout the matrix. The resulting blends were cast into a cylinder mold (D = 95 mm, h = 50 mm) and compacted following DIN 18127 with a compaction degree of 95 %. The samples were externally prepared by Ingenieurbüro Kügler in Essen, Germany. Each mixture was prepared in triplicate. Then, the prepared specimens were sealed in plastic bags and stored in a chamber at 20 °C and 90 % relative humidity for a curing period of 70d. For the carbonated samples, the specimens were transferred into a carbonation chamber with a 65 % relative humidity, 25 ± 0.1°C for one month. For the uncarbonated samples, the specimens were maintained in the previous chamber under the same curing conditions for one month.

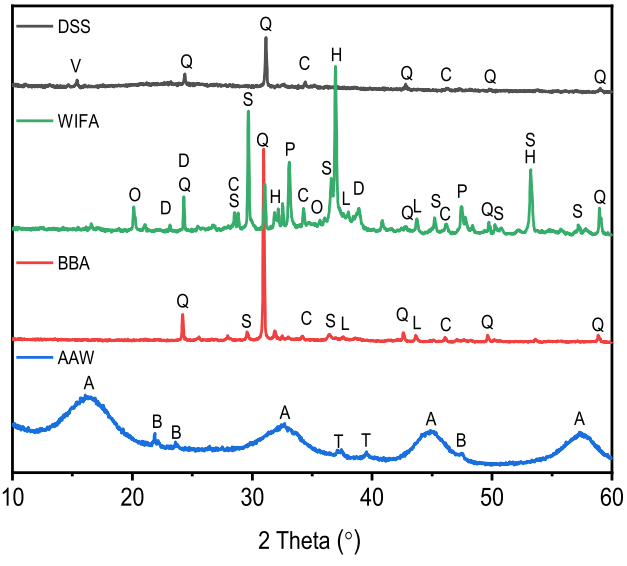

Fig. 1. XRD patterns of the raw materials. (A - boehmite: AlO(OH), B - bayerite: $Al(OH)_3$, C - calcite: $CaCO_3$, D - andradite: $Ca_3Fe_2(SiO_4)_3$, H - halite: NaCl, L - lime: CaO, V - vivianite: $Fe_3(PO_4)_2$•8 H_2O, O - Bassanite: $CaSO_4$•0.5 H_2O, P - potassium chloride: KCl, Q - quartz: SiO_2, S - anhydrite: $CaSO_4$, T - thenardite: Na_2SO_4).

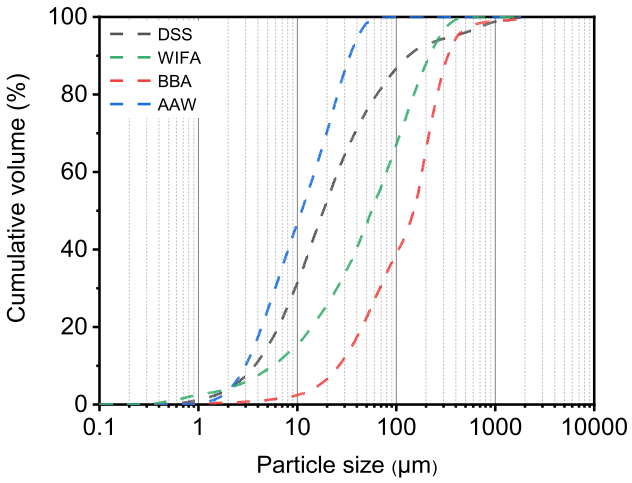

Fig. 2. Particle size distribution of each raw material.

Table 2
Formulations of the designed samples (wt%).

Group ID	Grain Fraction	DSS	WIFA	BBA	AAW	Additional WG (%)
DW1.5	45	46	9	0	0	1.5
DB1.5		46	0	9	0	
DA1.5		46	0	0	9	
DW2.0		46	9	0	0	2.0
DB2.0		46	0	9	0	
DA2.0		46	0	0	9	

DSS: digested sewage sludge, WIFA: waste incineration fly ash, BBA: biomass bottom ash, AAW: aluminum anodizing waste, and WG: waterglass.

2.3. Methodology

The flowchart of the investigation process is presented in Fig. 3.

2.3.1. Carbonation

The specimens were moved into a carbonation chamber (Memmert ICH260C). A circular airflow with 3 % CO_2 gas by volume was applied continuously during the test. The relative humidity was set to 65 %. Since few related parameters could be referenced from studies on the carbonation of landfill cover systems, the mentioned value was set according to the reported optimal value in the carbonation test for concrete and cement (Bernal et al., 2013; Leemann and Moro, 2017).

2.3.2. Permeability test

Permeability tests for both uncarbonated and carbonated samples were performed in accordance with DIN18130 and DIN EN ISO 17892. Cylindrical specimens were placed in pressure cells with side pressure, and permeability values were recorded every three days. The test was externally conducted by Ingenieurbüro Kügler in Essen, Germany.

2.3.3. Phase characterization

Following both the normal curing and carbonation curing, the phase assemblages of the prepared specimens were characterized through X-ray diffraction (XRD), Thermogravimetry (TG), and Fourier transform infrared spectroscopy (FT-IR). The specimens were slightly crushed and dried in a vacuum oven at 60 °C to remove the free water. The characterization was then performed on the powder samples (< 63 μm),

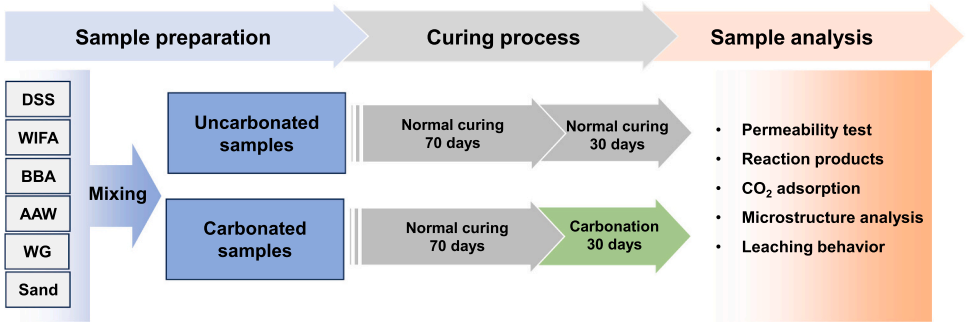

Fig. 3. Investigating the impact of carbonation on sludge-based sealing materials flowchart.

obtained through sieving the dried samples to remove coarse aggregates and concentrate the carbonated products. The XRD analysis was carried out by a Bruker D4 phaser, with a step size of 0.02° and a 2θ range from 10° to 60° (Co-Kα, 40 kV, 30 mA). The TG test was conducted by a STA 449 F1 instrument. The samples were heated from 40 °C to 1000 °C at a heating rate of 10 K/min under a N_2 atmosphere. For FT-IR analysis, a Varian 3100 instrument was employed to identify bonding in the mineral phases within the wavenumber range of 4000 – 400 cm^{-1}.

2.3.4. *Microstructure analysis*

N_2 sorption analysis of both uncarbonated and carbonated samples was conducted using Micrometrics Tristar II plus. The pore size distribution was determined at 77 K from the adsorption branch employing the Barrett – Joyner – Hallenda (BJH) method (Brunauer et al., 1938). The samples were pretreated by nitrogen gas flow with a heating rate of 10 K/min and heated at 60 °C for 24 h to remove moisture and impurities.

2.3.5. *Leaching behavior*

The leaching behavior of both uncarbonated and carbonated samples was analyzed using the one-batch leaching test (EN 12347–2). The cylindrical samples were crushed into small pieces (< 4 mm) and mixed with deionized water in polyethene bottles. These bottles were then sealed and placed horizontally on a linear reciprocating shaking device (Stuart SSL2) for 24 h shaking. The pH value of the leachate was initially measured using a pH meter and then acidified with HNO_3. The concentration of chloride (Cl^-) and sulfates (SO_4^{2-}) in leachates were analyzed by ion chromatography (Dionex 1100) equipped with an ion-exchange column AS9-HS. All other elements were quantified with inductively coupled plasma optical emission spectroscopy (ICP-OES Spectral Blue).

3. Results

3.1. *Permeability*

3.1.1. *Effect of different additives and waterglass dosage on the permeability of sealing materials*

The permeability of the specimens is evaluated using the k-value. Fig. 4 (a) shows the evolution of the k-values in the initial 75d for each uncarbonated specimen with 1.5 and 2.0 wt% waterglass. After the first 20d, the permeability value stabilizes, and the average value post this period is considered as its permeability value. Dutch legislation prescribes overall permeability limits of 6.34×10^{-10} m/s for the residue-based sealing layer materials (Rijkswaterstaat, 1991). The k-values of the investigated samples consistently fall below this threshold, ranging from 4.04×10^{-12} m/s to 6.48×10^{-10} m/s. This suggests the feasibility of using WIFA, BBA, and AAW in the preparation of landfill sealing materials with respect to permeability. AAW-modified specimens stand out with the lowest permeability. The reasons for this distinctive characteristic have been discussed in our previous study (Ling et al., 2024a),

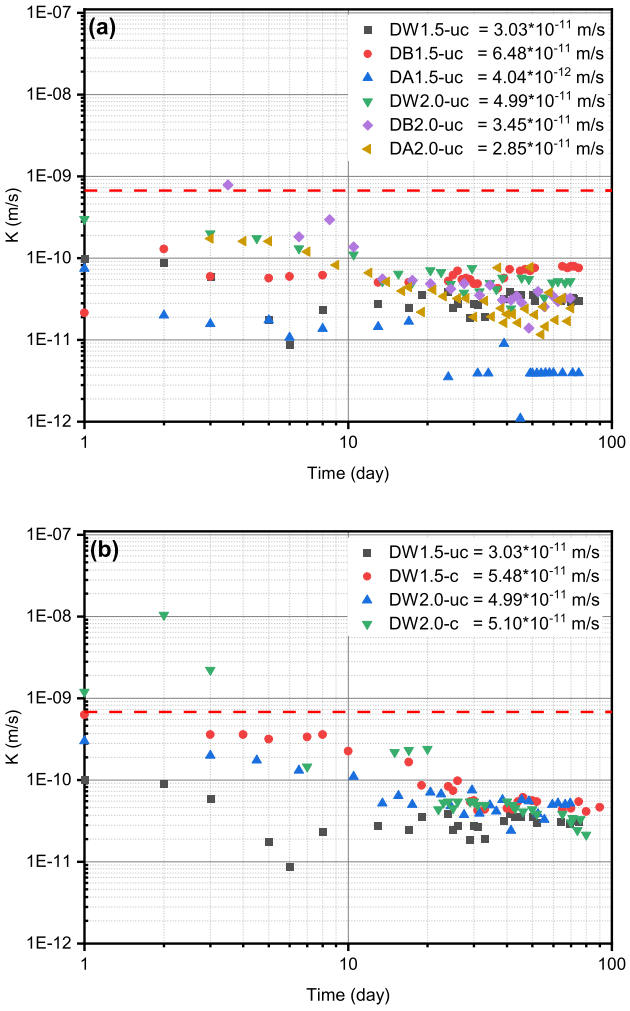

Fig. 4. The permeability test of the prepared samples within 75 days. (a): with different waterglass content and additives, (b): with (-c) or without (-uc) carbonation process for DW samples. Mixture details can be found in Table 2. The red line represents the maximum allowable k-value for landfill sealing materials according to Dutch legislation.

attributed to the finer particle size of AAW and the improved formation of gypsum that improves the packing system.

Furthermore, it is noteworthy that the waterglass dosage exerts varying effects on the permeability of the samples. Specifically, compared with DB1.5, the permeability of DB2.0 samples decreases with higher waterglass content. A plausible explanation for the observed decrease in permeability in DB2.0 is that the additional waterglass may

fill void spaces, thereby improving the overall packing system. Moreover, waterglass may contribute to the formation of other precipitates (gel products) that effectively reduce the porosity of the matrix, further contributing to the observed decrease in permeability. On the other hand, the permeability for DW2.0 and DA2.0 increases with more waterglass in comparison with that of DW1.5 and DA1.5. One potential reason could be the dissolution of inherent minerals within WIFA and AAW when mixing with waterglass, as the waterglass provides a localized strong alkaline environment. Specifically, boehmite in AAW could be dissolved as (Grénman et al., 2010; Tramontin et al., 2019):

$$AlOOH + OH^- + H_2O \rightarrow Al(OH)_4^- \quad (1)$$

This dissolution process may introduce pathways for fluid flow, consequently leading to higher permeability in AAW-modified samples.

3.1.2. Effect of carbonation on the permeability

The relatively lower CaO content in AAW makes it less vulnerable to the impacts of CO_2. Consequently, among the two remaining additives with relatively higher CaO content, WIFA was selected to assess its performance following carbonation. The effect of carbonation on the permeability of DW1.5 and DW2.0 is presented in Fig. 4(b). The k-value of DW1.5 experiences a substantial increase from 3.03×10^{-11} m/s to 5.48×10^{-11} m/s, indicating the formation of a higher pore volume post-carbonation. Upon the incorporation of 2 wt% waterglass, the permeability of DW2.0 remains largely unchanged, maintaining values between 4.99×10^{-11} m/s and 5.10×10^{-11} m/s. This suggests that the higher waterglass dosage reduces the degradation of the permeability caused by carbonation. One possible explanation is that waterglass facilitates the precipitation of silica gel, which remains unaffected by carbonation. Hence, the higher amount of precipitated silica gel from waterglass effectively obstructs the connective pores [36], thereby mitigating the adverse impact of carbonation. Fortunately, both DW1.5-c and DW2.0-c meet the requisite standards even after undergoing carbonation. Subsequent sections delve into the detailed mechanisms of permeability degradation in the specimens, exploring both micro-scale and macro-scale perspectives influenced by the carbonation process.

3.2. Phase changes

3.2.1. X-ray diffraction analysis (XRD)

To reveal the potential chemical reaction during the normal curing and carbonation process, the phase composition of the samples was characterized by XRD. Fig. 5(a) presents the XRD patterns of all samples containing 1.5 wt% waterglass. The uncarbonated samples, subjected to the same curing ages at ambient humidity, exhibit comparable XRD patterns, indicating a consistent phase composition. The identified crystalline phase include: gypsum ($CaSO_4 \bullet 2\,H_2O$, PDF#: 33–0311) characterized by diffraction peaks at $2\theta = 13.47°$, 24.11°, 33.94°, 36.28° and 38.92°, corresponding to d-spacings of 7.63Å, 4.28Å, 3.07Å, 2.87Å and 2.69Å, respectively; anhydrite ($CaSO_4$, PDF#: 72–0916), with peaks at $2\theta = 29.59°$ and 45.16° (d-spacing of 3.50Å and 2.33Å); calcite ($CaCO_3$, PDF#: 72–1937), exhibiting peaks at $2\theta = 34.24°$ and 46.05° (d-spacing of 3.03Å and 2.29Å); vivianite ($Fe_3(PO_4)_2 \bullet (H_2O)_8$, PDF#: 75–1186), identified by peaks at $2\theta = 15.31°$ and 21.13° (d-spacing of 6.72Å and 4.88Å); sodium chloride (NaCl, PDF#: 70–2509), with peaks observed at $2\theta = 36.96°$ and 53.27° (d-spacing of 2.82Å and 2.00Å); and quartz (SiO_2, PDF#: 89–8935), displaying peaks at $2\theta = 24.23°$ and 31.00° (d-spacing of 4.26Å and 3.35Å). The formation of gypsum within the sealing materials is associated with the soluble sulfate and calcium content from raw materials (see supplementary materials Table S.1). It should be noted that the presence of anhydrite could be attributed to the transformation of the gypsum during the drying process of the XRD sample preparation. The primary distinction among the uncarbonated samples modified with BBA, WIFA or AAW lies in the varied intensity of gypsum, attributed to the distinct sulfate content in the raw additives (as summarized in Table 1). For the carbonated samples, no significant changes are observed in DB1.5-c and DA1.5-c compared to DB1.5-uc and DA1.5-uc in terms of phase composition. However, visible alterations occur in DW1.5-c, where distinct peaks at $2\theta = 19.50°$, 23.88°, 44.35°, 48.88° and 55.28° (corresponding to d-spacing of 5.28Å, 4.32Å, 2.37Å, 2.16Å and 1.93Å) appear, indicating the formation of monohydrocalcite ($CaCO_3 \bullet H_2O$ PDF#: 84–0049). The formation of monohydrocalcite entails the consumption of calcite, accompanied by the absorption of a portion of free water from the matrix, which becomes chemically bound within the monohydrocalcite structure. Nonetheless, the amount of this bound water is assumed to be minimal, given the minor intensity of monohydrocalcite formation.

Upon the incorporation of 2 wt% waterglass, the XRD patterns for all samples, both with and without carbonation, are depicted in Fig. 5(b). The higher dosage of waterglass has no discernible influence on the phase composition of the mixture. Meanwhile, the formation of monohydrocalcite is evident in the DW2.0-c as well.

3.2.2. Thermogravimetric analysis (TGA)

To quantify the amount of formed gypsum, monohydrocalcite and calcite, both uncarbonated and carbonated samples were subjected to Thermogravimetric analysis. Fig. 6 illustrates the TG and DTG curves of all prepared samples. For the uncarbonated samples, major mass losses are observed at approximately 135 °C, 265 °C, and 750 °C. These are attributed to the dehydration of gypsum (Paulik et al., 1992), the decomposition of organic content originating from the sewage sludge (Olszak-Humienik, 2001) (see TG and DTG results of raw DSS in

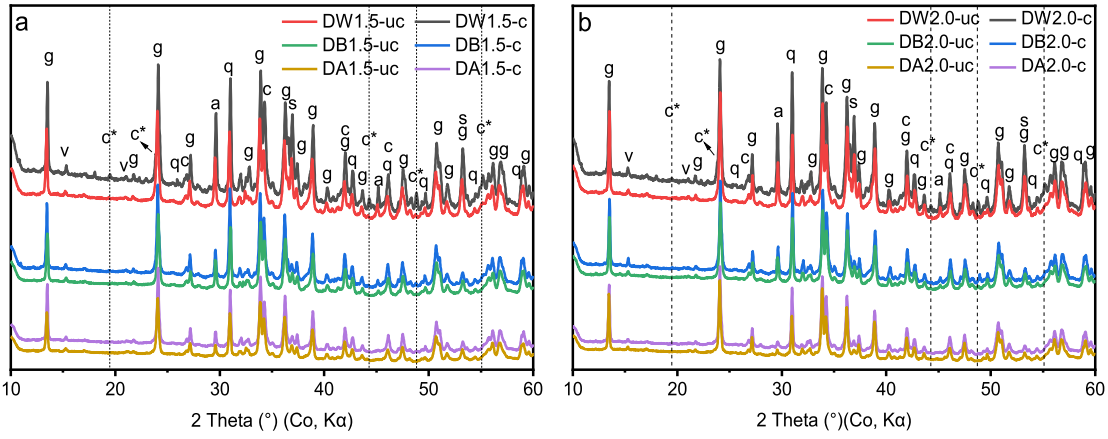

Fig. 5. XRD patterns of the powder samples in each group with (-c) or without (-uc) carbonation. (a - Anhydrite: $CaSO_4$, c - Calcite: $CaCO_3$, c* - Monohydrocalcite: $CaCO_3 \bullet (H_2O)$, g - Gypsum: $CaSO_4 \bullet 2\,H_2O$, q - Quartz: SiO_2, s - Sodium chloride: NaCl, v - Vivianite: $Fe_3(PO_4)_2 \bullet (H_2O)_8$).

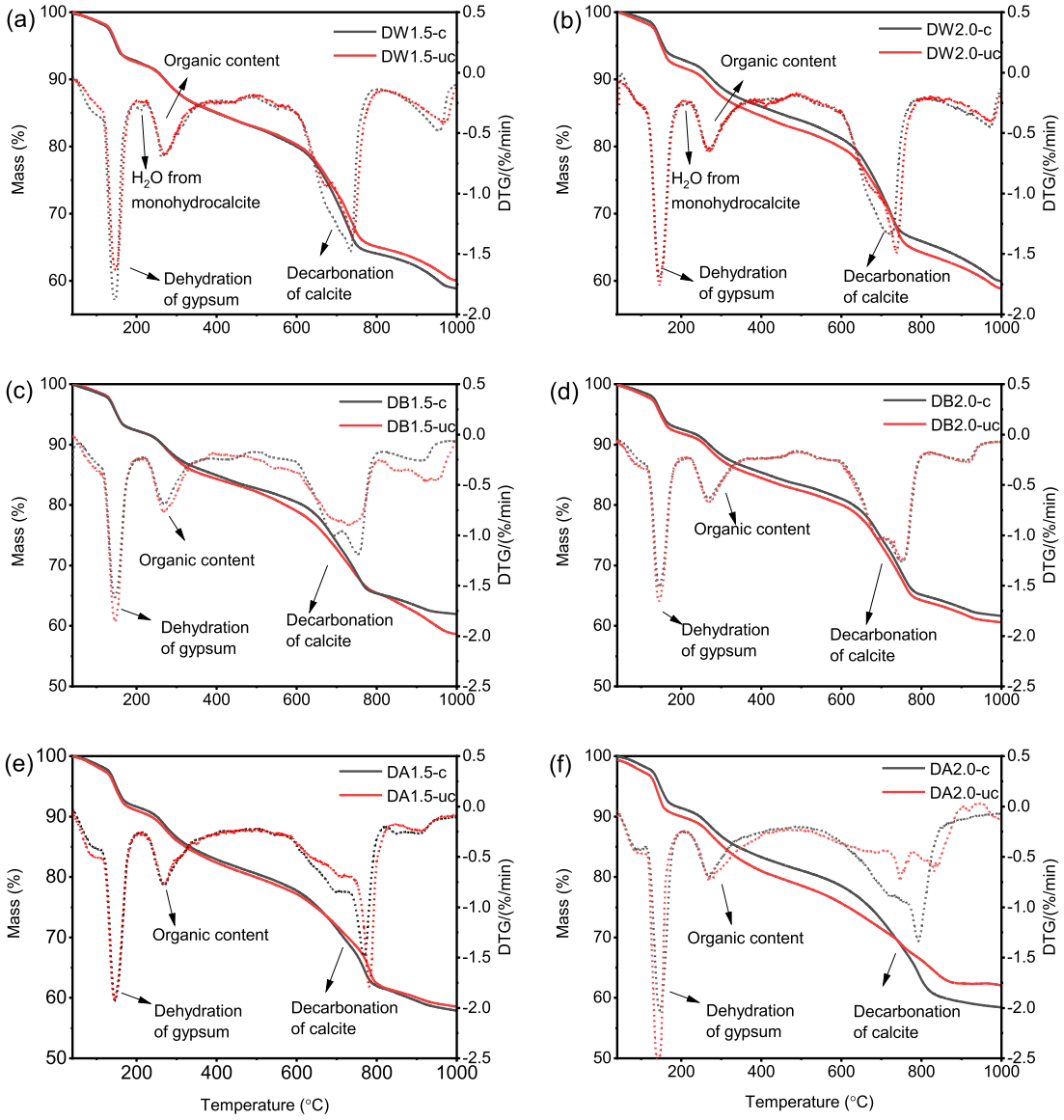

Fig. 6. TG-DTG curves of each sample with (-c) or without (-uc) carbonation. (a): DW1.5, (b): DW2.0, (c): DB1.5, (d): DB2.0, (e): DA1.5, and (f): DA2.0. Mixture details can be found in Table 2.

supplementary Figure S.1), and the decarbonation of calcite (Rodriguez-Navarro et al., 2009), respectively. Similar mass losses can be observed in the carbonated samples. Interestingly, there is minimal variation in the curves representing organic content from the sludge, indicating its stability during the carbonation process. However, some differences are highlighted in the mass loss due to the dehydration of gypsum and the decarbonation of calcite. Hence, their specific mass loss was calculated using the tangential method (Scrivener et al., 2016), with the results summarized in Table 3. It should be noted that the thermal decomposition of monohydrocalcite and gypsum occurs within

Table 3
Mass loss calculation at different temperature ranges based on the TG results (wt%).

Group	Bound water Temperature range (110–200°C)				Decarbonation of carbonates Temperature range (600–800°C)			
	Without Carbonation-(uc)	Std*	With Carbonation-(c)	Std	Without Carbonation-(uc)	Std	With Carbonation-(c)	Std
DW1.5	5.9	0.31	5.6 (0.8) **	0.26 0.03	15.2	0.21	15.8	0.27
DB1.5	5.5	0.09	5.8	0.11	14.8	0.19	15.1	1.05
DA1.5	6.3	0.22	6.2	0.12	15.6	0.06	16.5	0.12
DW2.0	6.2	0.01	5.5 (0.8) **	0.04 0.07	15.6	0.03	15.6	0.30
DB2.0	5.8	0.09	5.5	0.11	15.8	0.05	15.9	0.10
DA2.0	6.8	0.21	6.5	0.10	15.7	1.52	17.6	0.12

Std* represents the standard deviation. ()** represents the mass loss due to the dehydration of monohydrocalcite from DW1.5-c and DW2.0-c.

overlapping temperature ranges (typically 150 – 240°C), making full deconvolution of mass loss challenging. In this study, fixed temperature intervals were applied to approximate their respective contributions: 115 – 190°C for gypsum dehydration and 190 – 230°C for monohydrocalcite dehydration. While this approach may underestimate the mass loss attributable to monohydrocalcite dehydration, it provides a reasonable basis for its identification and for comparing relative formation levels across samples.

The analysis of bound water content reveals variations in gypsum formation depending on the additives used, particularly with higher sulfate content in AAW resulting in increased gypsum formation in DA1.5 and DA2.0. However, comparing bound water in uncarbonated and carbonated samples shows only slight differences, suggesting a slight decrease in gypsum production. This decrease may be attributed to the consumption of calcium ions during the carbonation curing process. To visualize the potential effect on pore volume induced by this phase transition, theoretical chemical deformation was calculated based on literature data (Churio et al., 2003; Duedall, 1972; Li et al., 2019; Serafeimidis and Anagnostou, 2014; Singman, 1984; Turnbull, 1973), resulting in a chemical deformation of −0.010 ml/g_{gypsum}, as summarized in Table 4. Considering the minor changes observed in bound water, possibly influenced by sample variability, and the effectiveness of normal curing phases in facilitating significant gypsum formation (Ling et al., 2024a), it can be inferred that the carbonation process has minimal impact on pore volume due to gypsum production variations. Meanwhile, confirmation of monohydrocalcite formation in DW1.5-c and DW2.0-c was achieved through the detection of a tiny peak around 200 °C (Yao and Zhou, 2015). The chemical deformation resulting from monohydrocalcite formation was calculated to be −0.062 ml/$g_{calcite}$. This further supports the conclusion that while the formation of monohydrocalcite contributes to chemical deformation, its impact on the matrix porosity is limited.

Additionally, different groups of samples exhibit varying degrees of calcite increase post-carbonation. The associated chemical deformation, quantified at −0.073 ml/$g_{calcite}$, is relatively significant, indicating that calcite formation through carbonation is the primary driver of the increase in porosity. Despite the anticipation that higher CaO content in the raw materials would lead to greater CO_2 adsorption, DW samples and DB samples exhibit relatively low CO_2 uptake within the fine fraction (< 63 μm) compared to DA samples. Although BBA and WIFA release higher amounts of Ca ions in their leaching test, XRD analysis (Fig. 1) indicates that in WIFA, the leached Ca is mainly derived from bassanite, gypsum and lime, while in BBA, it comes primarily from anhydrite and lime. Since lime is more reactive with CO_2 than bassanite and gypsum, it contributes more significantly to CO_2 uptake. The observed low CO_2 uptake in DW and DB suggests a low lime content, which is consistent with the low degradation of impermeability. It is also essential to consider potential sources of experimental uncertainties in TGA, such as sampling inconsistencies and unintended carbonation during preparation, which could influence the observed CO_2 uptake. To address variability, all measurements were conducted in duplicate, and average values were reported with standard deviations. Interestingly, DA1.5-c and DA2.0-c show a relatively high increase in CO_2 adsorption rates. Li et al. (2023) have revealed that hierarchical porous AlOOH hollow microspheres can improve CO_2 capture, and a similar mechanism may apply to the amorphous AlOOH in AAW, which exhibits a porous structure as confirmed by the BET analysis in Fig. 8. However, the potential for enhanced CO_2 uptake by AAW remains speculative, based on its structural characteristics and supporting literature. Further direct CO_2 adsorption testing is necessary to validate this function of AAW. Overall, the CO_2 adsorption capacity of the sealing materials is relatively low, especially in DW groups, accounting for the low degradation of impermeability post-carbonation.

Table 4
Calculation of chemical deformation due to the formation of calcite and monohydrocalcite.

Reactants/Reaction products	Moles	Mass (g)	Molar volume (ml/mol)	Volume (ml)
$CaSO_4{\cdot}2\,H_2O$	1	172.17	74.3 (Serafeimidis and Anagnostou, 2014)	74.3
H_2O	2	18.2	18.0 (Li et al., 2019)	36.0
SO_4^{2-}	1	96.06	13.9 (Churio et al., 2003)	13.9
Ca^{2+}	1	40.08	26.20 (Singman, 1984)	26.20
Volume change due to gypsum formation			−1.8 ml	
Chemical deformation			−0.010 ml/g gypsum	
$CaCO_3$	1	100.09	36.9 (Duedall, 1972)	36.9
H^+	2	1	0 (Myers et al., 2014)	0
Ca^{2+}	1	40.08	26.20 (Singman, 1984)	26.20
H_2O	1	18.02	18.0 (Li et al., 2019)	36.0
Volume change due to calcite formation			−7.3 ml	
Chemical deformation			−0.073 ml/g calcite	
$CaCO_3$	1	100.09	36.9 (Duedall, 1972)	36.9
H_2O	1	18.2	18.0 (Li et al., 2019)	18.0
$CaCO_3{\cdot}H_2O$	1	118.10	48.7 (Turnbull, 1973)	48.7
Volume change due to monohydrocalcite			−6.2 ml	
Chemical deformation			−0.062 ml/g calcite	

3.2.3. Fourier transform infrared spectroscopy (FT-IR)

Fig. 7 presents the FT-IR spectra of the investigated samples, both with and without carbonation. The observed broad bands around 3528–3405 cm^{-1} and 1684–1614 cm^{-1} are ascribed to the stretching and bending vibrations of the H–OH bond in gypsum, respectively (Böke et al., 2004). The peaks around 1112 cm^{-1}, 667 cm^{-1}, and 596 cm^{-1} are assigned to the stretching and bending modes of sulfate in gypsum or anhydrite (Chukanov, 2014). The absorption peaks at 1411 cm^{-1} and 871 cm^{-1} originate from the vibration of ν_3 [CO_3^{2-}] and ν_2 [CO_3^{2-}] from the calcite and monohydrocalcite, respectively. The increased intensity of these two adsorptions after the carbonation process also confirms the heightened carbonate formation.

Additionally, the adsorption peak observed around 1026 cm^{-1} can be attributed to the Si-O-Si vibrations (Huang et al., 2025; Li et al., 2017). Hua et al. (2010) have proposed the reaction of waterglass in the presence of gypsum, as shown by:

$$CaSO_4 + Na_2O \bullet nSiO_2 \rightarrow CaO \bullet nSiO_2 + Na_2SO_4 \quad (2)$$

Since FT-IR primarily detects bond vibrations, it is challenging to distinguish whether the Si-O-Si peak arises from waterglass or calcium silicate gel. It is important to note that the calcium silicate gel is sensitive to the carbonation process and will undergo further decomposition with the formation of calcite and silicate gel (Cheng et al., 2024; Song et al., 2014). After carbonation, a noticeable shift of the Si-O-Si peak toward higher wavenumbers is observed (Fig. 7), which has been attributed to the silicate gel formation, consistent with previous studies on carbonated alkali-activated materials (Li et al., 2017). In conclusion, the additional waterglass participates in the formation of silicate gel in the final carbonated samples. This implies that a higher dosage of waterglass results in a greater formation of silicate gel, which may account for the lower permeability obtained after carbonation due to the filler effect of silicate gel within the matrix. It is worth noting that, due to the amorphous nature of silica gel, its formation is not detectable in the previous XRD patterns (Cheng et al., 2025).

3.3. Physical changes

3.3.1. Microstructure

The permeability of sealing materials is notably influenced by their

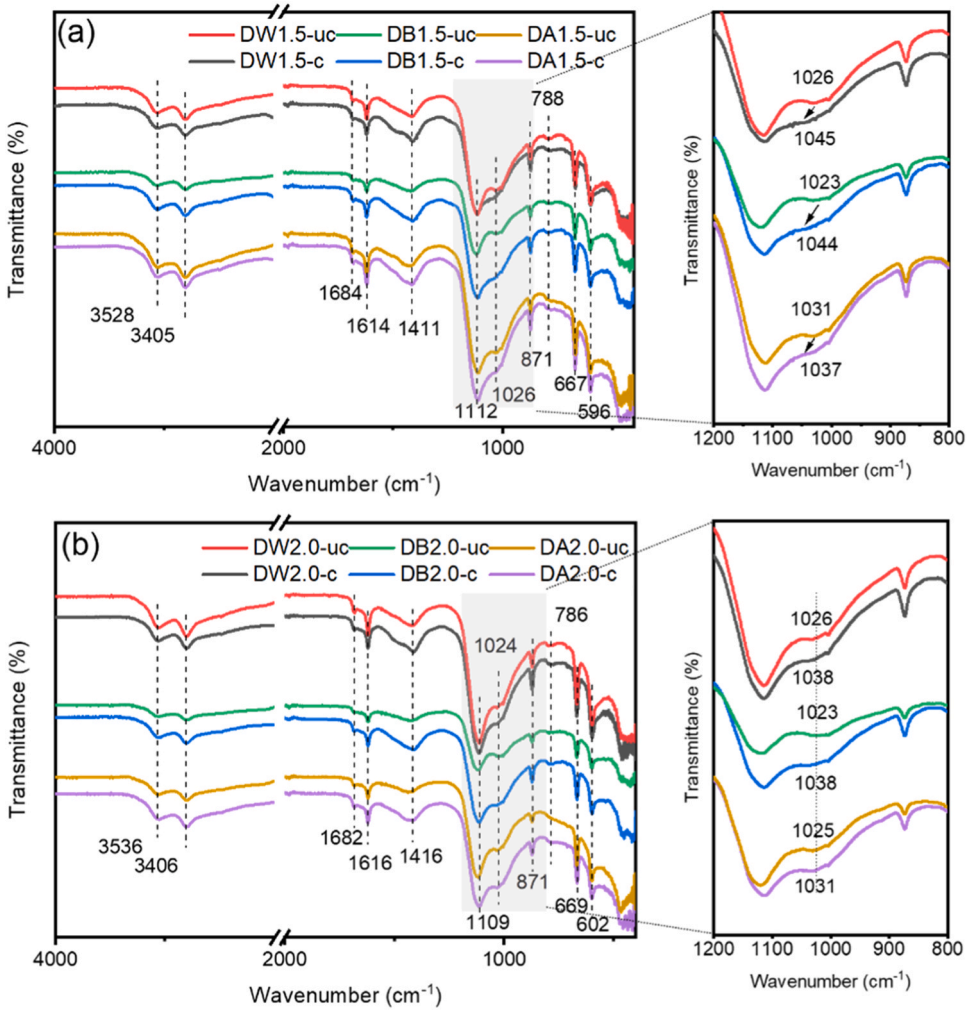

Fig. 7. FT-IR spectra of each sample with (-c) or without (-uc) carbonation.

microstructure, with pores creating pathways for fluid flow. To assess the impact of the carbonation process on the microstructure, N_2 adsorption analysis was conducted on both the samples and raw additive materials. Following the International Union of Pure and Applied Chemistry (IUPAC) classification, pores are categorized as micropores (< 2 nm), mesopores (2 – 50 nm) and macropores (> 50 nm) based on their pore size (Sing, 1985). The application of the BJH method in N_2 adsorption analysis is recommended for determining mesopores (Zhang and Scherer, 2019). Within the mesopores range, two primary classes are identified: gel pores (2 – 10 nm) and capillary pores (10 – 50 nm) (Ma et al., 2013). The pore size distribution for each sample was calculated, and the results are illustrated in Fig. 8.

The pore size distribution in the samples with normal curing is predominantly influenced by the additives employed. Specifically, the AAW-modified samples demonstrate high volumes of gel and capillary pores. This tendency is linked to the presence of low crystalline boehmite, as confirmed by XRD presented in Fig. 1. The higher gel content in AAW contributes to the lower permeability observed in AAW-modified samples, as illustrated in Fig. 4. In contrast, other additives contribute minimally to the volume of gel and capillary pores. Upon applying a higher dosage of waterglass, both pores and capillary pores in AAW-modified samples increase, with limited impact on other samples. This phenomenon is attributed to the dissolution of boehmite within AAW in an alkaline environment, as proposed in Eq. (1). Additionally, this observation elucidates the rationale behind the increased permeability of AAW-modified samples with higher waterglass dosage.

In the carbonated samples, a notable reduction in gel pores and capillary pores is observed in AAW-modified samples (DA1.5-c and DA2.0-c) after carbonation, whereas minimal changes are noted in other samples. The decrease in pore volume may stem from the "pore blocking" effect resulting from the formation of carbonates (Morandeau et al., 2015). Additionally, a higher dosage of water induces an increase in gel pore volume due to the formation of silicate gel.

3.3.2. *Macro-scale change*

After the carbonation process, a significant mass loss was observed in all specimens. This can be attributed primarily to the evaporation of free water during the carbonation and the decalcification of gypsum due to the carbonation process. Moreover, based on the XRD and TG analysis, the absorbed CO_2 during the carbonation curing plays a crucial role in forming carbonates and the formation of monohydrocalcite also contributes to the bonding of free water in the matrix. To illustrate the complexities of these mass changes, a schematic representation is presented in Fig. 9 (a). Subsequently, the calculation of CO_2 adsorption and newly bonded water in each mixture was carried out in accordance with the formulations presented by:

$$M_t = M_{uc} - M_c \tag{3}$$

$$M_w = M_{uc} \times w_{uc} - M_c \times w_c \tag{4}$$

$$\alpha_{(CO_2 \ + \text{bound water})} = \frac{M_w - M_t}{M_{uc}} \tag{5}$$

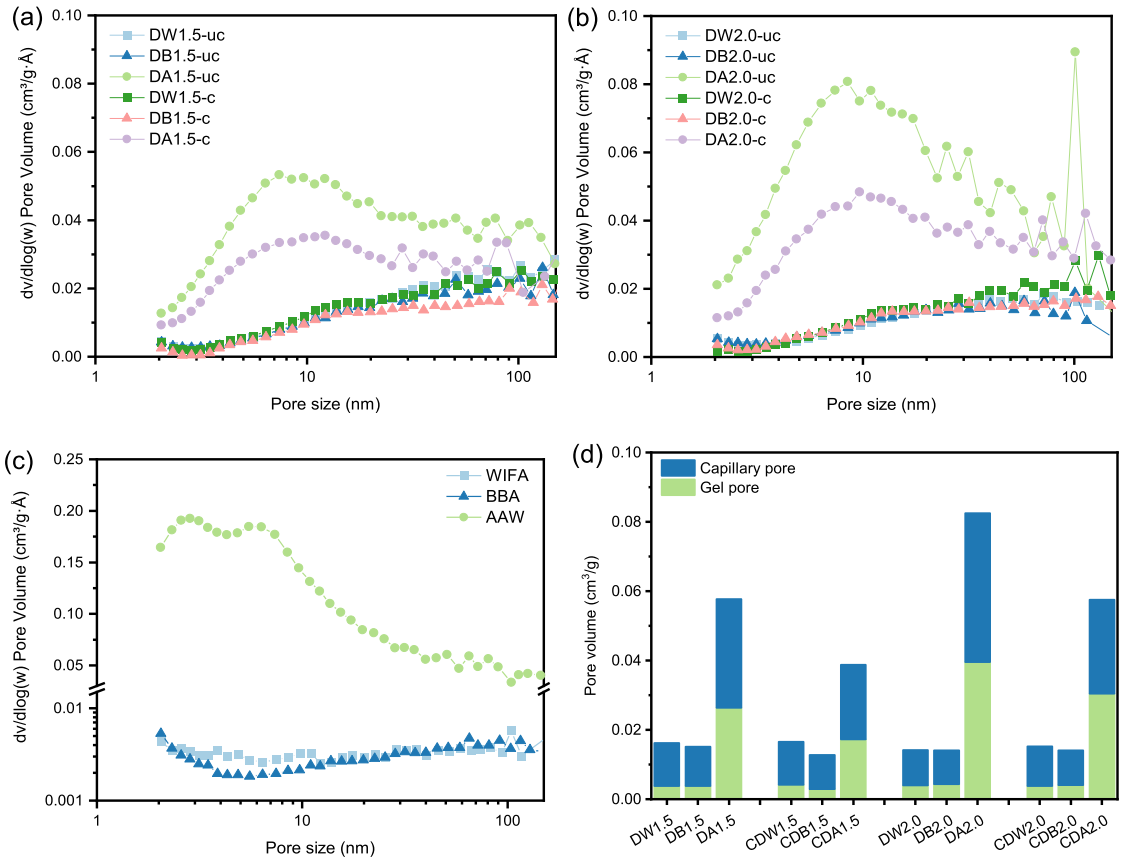

Fig. 8. Pore size distribution of each sample from BJH adsorption: (a) samples with 1.5 wt% waterglass, (b) samples with 2.0 wt% waterglass, (c) raw WIFA, BBA and AAW, (d) cumulative pore volume of capillary pore and gel pore. Mixture details can be found in Table 2.

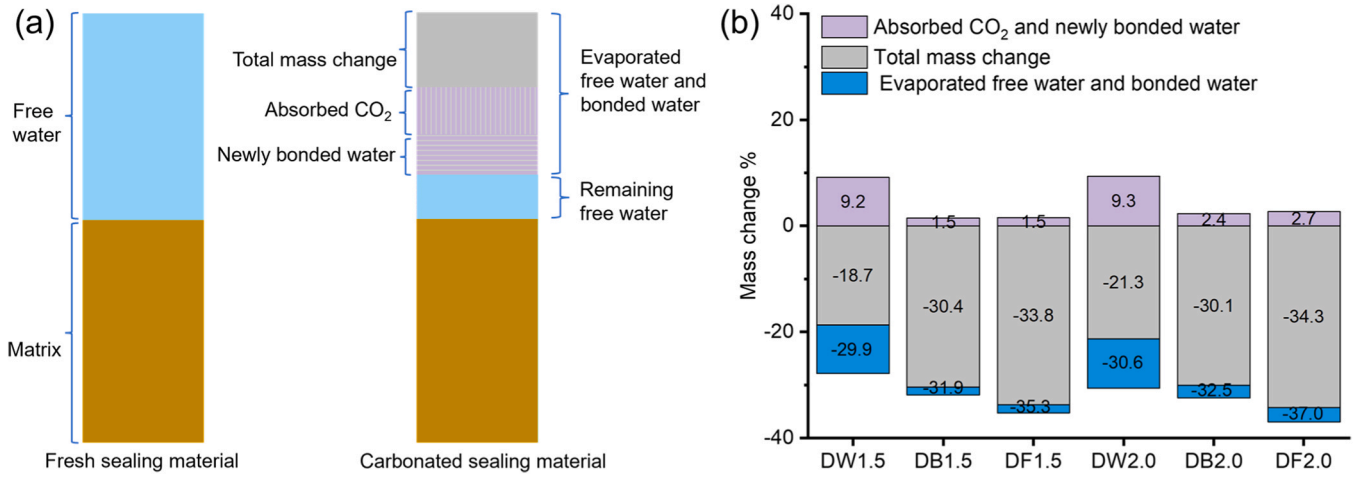

Fig. 9. (a) schematic of mass changes within the matrix (b) calculation of the mass change in each carbonated sample. (The negative values mean the mass loss of the matrix).

where α is the total CO_2 and bound water adsorption rate for each mixture, w_{uc} and w_c denote the moisture content from the uncarbonated and carbonated samples, respectively. Similarly, M_{uc} and M_c correspond to the total mass of the uncarbonated and carbonated samples, while M_w is the mass of the evaporated free water and M_t is the total mass change.

The results in Fig. 9 (b) indicate that the overall mass change in the specimens is primarily associated with the chosen additives. Specifically, samples from the DW group exhibit a higher mass change in the overall adsorption of CO_2 and bound water. This outcome is ascribed to the augmented formation of monohydrocalcite within the DW group, as evidenced by the TG and DTG results in Fig. 6, resulting in higher bound water content. The application of a higher dosage of waterglass slightly amplifies each mass change, likely attributed to the presence of free water within the waterglass and its reaction with minerals, resulting in the formation of hydrates.

3.4. Environmental impact

In addition to permeability, the leaching behavior of sealing materials represents a crucial consideration, particularly in mitigating soil pollution risks. Despite the common implementation of leachate collection systems in contemporary landfill infrastructure, the propensity for leaching in sealing materials subsequent to carbonation warrants thorough investigation (Rubinos and Spagnoli, 2018). In this study, we present the design and evaluation of sludge-based landfill sealing materials, with a particular focus on elucidating the leaching behavior of both uncarbonated and carbonated samples. Through systematic analysis, we aim to assess the potential environmental implications associated with these materials comprehensively.

Table 5 presents the leaching results obtained from both uncarbonated and carbonated samples. The leaching behavior of the formulated sealing materials is notably influenced by the carbonation process. Specifically, the leaching of various elements increases in the carbonated specimens, including chloride, cadmium, copper, nickel, lead, antimony, zinc, sodium, potassium, iron, and magnesium, aligning with findings from previous studies highlighting augmented leaching quantities of these elements in carbonated samples (Alba et al., 2001; Shafique et al., 1998; Valls and Vàzquez, 2001). Of significance is the contrasting leaching behavior observed for certain elements, particularly sulfate and calcium, which show decreased leaching. The potential reason for the reduced sulfate leaching is the reaction with the above heavy metal ions, leading to the precipitation, while for Ca, it is the chemical binding within calcite or carbonates (Sanchez et al., 2002).

Compared with the permissible emission limits regulated by Council Decision 2003/33/EC (Council, 2002), only the leaching levels of chloride and antimony in the DW group exceed the prescribed limits. This high leaching of these elements can be traced back to the raw WIFA component (see Supplementary Table S.1). Since chloride and antimony are leachable from WIFA, a pre-treatment, such as a washing process, may be necessary and is recommended before their use in the formulation of sealing materials. Overall, the potential for heavy metal pollution due to leaching after the carbonation of the designed landfill sealing materials appears to be limited. The formulated DB and DA groups show promise as viable alternatives for preparing landfill sealing materials, as they do not impose additional burdens on leachate treatment. Additionally, the leaching behavior of these sealing materials is influenced by the specific additives used, indicating that when other industrial by-products are considered, their leaching performance should be carefully evaluated to minimize additional leachate treatment costs.

4. Discussions

4.1. Carbonation mechanism of sealing materials

In this study, an accelerated carbonation process has been utilized to investigate the impact of CO_2 released from decomposed organic waste in landfills on the permeability of sealing materials. Despite the low permeability of the formulated sealing materials, the diffusion of CO_2 within the matrix is inevitable. Subsequently, the degradation mechanism of impermeability is elucidated from both the chemical and physical perspectives. Firstly, in the landfill sealing materials, a certain amount of moisture is indispensable as it acts as a lubricant during compaction, facilitating the tight rearrangement of particles. Importantly, the presence of moisture enables the dissolution and subsequent carbonation of leachable calcium ions, especially in CO_2-rich environments, as expressed by:

$$Ca^{2+} + CO_2 + H_2O = CaCO_3 + 2H^+ \quad (6)$$

It is essential to note that, based on XRD results, several calcium-bearing phases are present, which have higher solubility compared to calcite. Consequently, under conditions of sufficient CO_2, calcite precipitation can occur. The volume disparity between these two phases leads to a reduction in solid-phase volume within the pores, which indirectly contributes to an increase in pore size. This process is elaborated in Fig. 10, illustrating the increase in capillary pores caused by the aforementioned carbonation reaction, aligning with the findings presented in Fig. 8. Additionally, during the dissolution of gypsum, bound water is released, leading to an increase in free water content within the capillary pores, consistent with the tend observed in Fig. 9.

It is also noteworthy that, when considering the diverse additives within the sealing materials, the formation of monohydrocalcite is significantly more pronounced in WIFA-modified samples. Nishiyama et al. (2013) have demonstrated that the monohydrocalcite formation typically necessitates its surroundings to be saturated with magnesium carbonate to prevent its dehydration to anhydrous calcium carbonate. A similar equilibrium between monohydrocalcite and magnesium carbonate is likewise observed in some saline lakes (Nishiyama et al.,

Table 5
Leaching results of uncarbonated and carbonated specimens (mmol/kg of dry raw material).

Elements	DW1.5		DB1.5		DA1.5		DW2.0		DB2.0		DA2.0		Limit*
	uc	c	uc	c	uc	c	uc	c	uc	c	uc	c	
Cl^-	420.1	508.2	164.6	210.9	150.8	216.8	767.5	507.7	174.5	219.7	125.8	106.2	422.5
SO_4^{2-}	86.86	79.45	75.17	76.96	103.1	85.91	151.5	98.95	99.80	89.46	147.9	128.5	208.3
As	0.009	0.006	0.007	0.009	0.004	0.007	0.011	0.008	0.010	0.012	0.006	0.009	0.027
Ba	0.002	0.002	0.001	0.001	0.001	0.001	0.002	0.002	0.001	0.001	0.001	0.001	0.728
Cd	0.002	0.007	-	-	-	-	0.002	0.004	-	-	-	-	0.009
Cr	-	0.001	-	0.001	-	-	-	-	-	0.001	-	-	0.192
Cu	0.077	0.152	0.007	0.110	0.003	0.029	0.050	0.230	0.027	0.079	-	0.013	0.787
Mo	0.026	0.016	0.016	0.017	0.010	0.014	0.030	0.024	0.014	0.018	0.005	0.010	0.104
Ni	0.005	0.007	0.005	0.009	0.004	0.008	0.006	0.011	0.005	0.009	0.008	0.012	0.170
Pb	0.011	0.013	0.015	0.017	0.009	0.020	0.012	0.021	0.012	0.022	0.020	0.023	0.048
Sb	0.009	0.012	0.003	0.004	0.004	0.005	0.012	0.015	0.005	0.005	0.002	0.002	0.006
Zn	0.015	0.038	0.011	0.019	0.007	0.017	0.020	0.044	0.008	0.025	0.002	0.012	0.765
Na	351.8	392.1	164.8	221.7	182.3	262.6	624.1	430.1	199.7	252.0	231.1	235.8	
K	113.7	121.5	43.61	53.60	31.08	43.69	180.8	116.6	45.37	54.17	24.16	22.69	
Ca	29.99	20.20	20.04	15.17	20.05	14.67	52.61	20.82	24.06	15.54	24.21	12.23	
B	0.441	0.390	0.445	0.385	0.412	0.457	0.546	0.447	0.445	0.382	0.545	0.417	
Fe	0.004	0.006	0.004	0.012	0.002	0.006	0.005	0.008	0.004	0.016	0.003	0.011	
Li	0.691	0.668	0.616	0.438	0.593	0.511	0.904	0.649	0.861	0.424	0.866	0.469	
Mg	21.11	24.50	13.58	15.93	12.62	16.52	22.73	27.19	16.77	17.21	11.45	12.06	
Sr	0.082	0.081	0.051	0.043	0.056	0.044	0.088	0.076	0.059	0.045	0.061	0.039	
pH	8.20	8.07	8.16	8.05	8.22	8.07	8.26	8.21	8.19	8.05	8.36	7.99	

uc = Uncarbonated sample, c = Carbonated sample. * - The Council Decision 2003/33/EC limits (Council, 2002). Underlined values are above the limits.

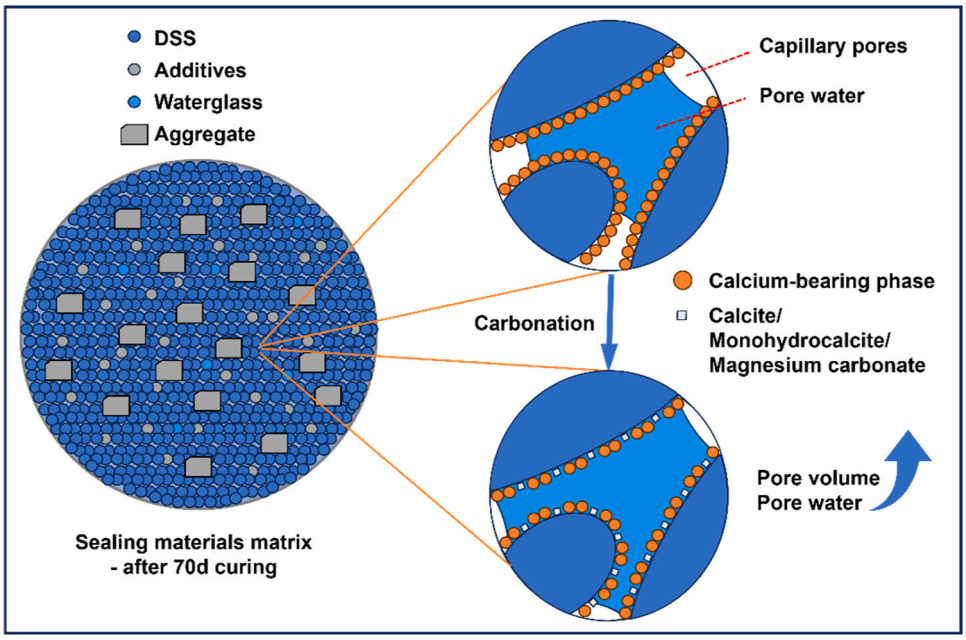

Fig. 10. Schematic diagram of microstructure changes of sealing materials under carbonization effect.

2013). Consistent with these findings, the relatively high leachable magnesium content from WIFA (see supplementary Table S.1) accounts for the marked formation of monohydrocalcite in the WIFA-modified samples, as opposed to the BBA-modified samples. Moreover, the increased leachable magnesium ions give rise to the formation of magnesium carbonates. This is evidenced by the prominent peak at 2θ = 38.11° (d-spacing of 2.74Å) for magnesium carbonates in XRD patterns of the carbonated DW samples, as depicted in Fig. 11. Therefore, the contents of soluble calcium and magnesium ions in the additive are crucial factors influencing carbonation products. Nevertheless, current results indicate that the impermeability of the WIFA-modified group after carbonization meets the requirements, suggesting a threshold for calcium and magnesium ions. Quantitative investigation into the impact of calcium and magnesium ion contents in the additive on the impermeability degradation after carbonization should be further conducted to facilitate standardized selection criteria of additives.

4.2. Limitations of the accelerated carbonation process

Due to the limited availability of relevant studies examining the potential impact of released CO_2 on the permeability of sealing materials, we have to choose an accelerated carbonation process commonly used in cement systems (Gunning et al., 2010; Ling et al., 2024c). However, it is imperative to underscore certain differentiating aspects between accelerated carbonation and the natural carbonation process within this context. The principal distinguishing factors are outlined in Fig. 12, encompassing gas types and concentrations, temperature, infiltration paths and free water evaporation. In the natural carbonation process, the simultaneous generation of CO_2 and CH_4 occurs during the biodegradation of organic waste materials. This biodegradation process leads to an escalation in greenhouse gas concentrations. Furthermore, the resultant exothermic chemical reactions frequently induce an elevated temperature within conventional landfill environments (Sabrin et al., 2020). Studies have indicated temperature escalations from ambient levels to 38 °C ~ 54 °C after years of closure (Jafari et al., 2017). Additionally, because of the stratified configuration of the landfill cover system, gas migration predominantly occurs upward solely from the bottom surface during the natural carbonation process, differing from its diffusion pattern emanating from the perimeter towards the center in the accelerated carbonation process. Lastly, evaporation of sealing materials is inevitable within the carbonation chamber, whereas the sealing layer exhibits limited evaporation of free water as an internal layer in a compacted cover system. However, the influence of these differences on carbonation outcomes primarily resides in the rate at which carbonation penetrates, with fewer impacts on the composition and structure of the carbonation post-application. Free water evaporated from the surface will be replenished during the permeability test, rendering the observed permeability degradation in the experimental findings reliable. Overall, the decreased impermeability of the sealing materials (see Fig. 4) still complies with the requirements outlined in Dutch legislation concerning residues-based sealing materials used for landfill cover systems (Rijkswaterstaat, 1991). It should be noted that for an effective assessment of the long-term service viability of sealing materials, constructing an improved carbonation model that aligns with the actual carbonation process would be recommended, facilitating a more precise evaluation.

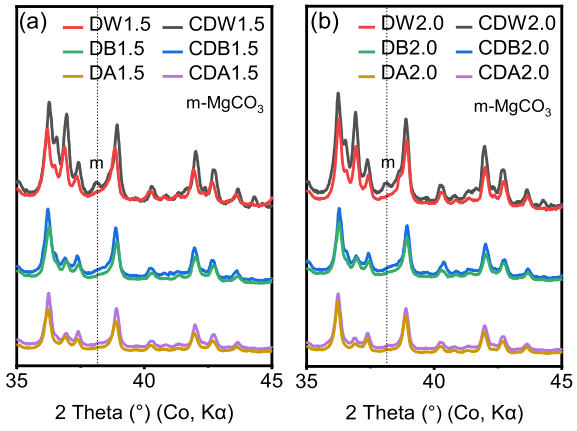

Fig. 11. The XRD pattern of all samples with 2 Theta range of 35° to 45° (m: $MgCO_3$ – PDF# 086–2346).

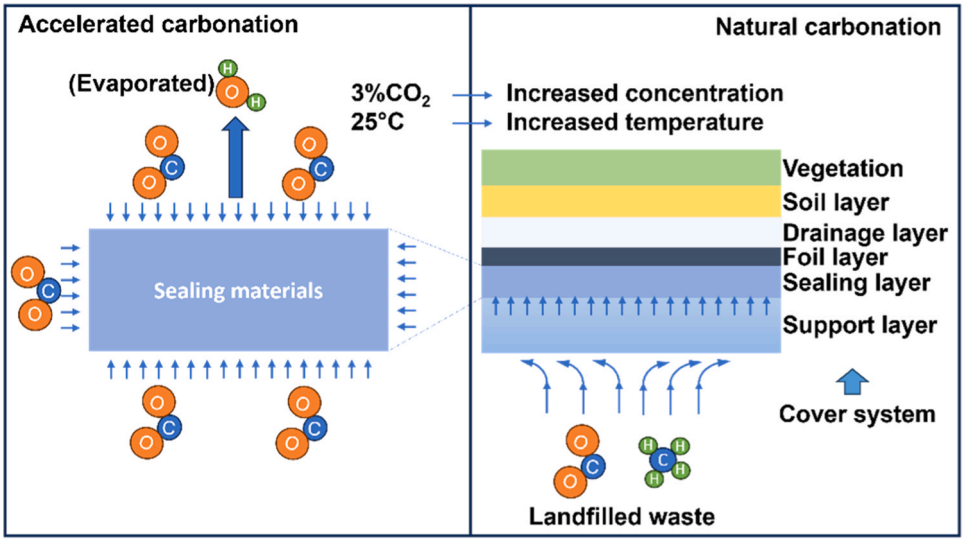

Fig. 12. Comparison of accelerated carbonation process and natural carbonation process.

4.3. The effect of waterglass and various additives on the sealing materials

Previous studies have highlighted the critical role of waterglass as a bonding agent in reducing the permeability of sealing materials (Boels et al., 2005). However, the recycling and utilization of industrial solid wastes as additives and their potential interactions with waterglass remain insufficiently investigated. To address this gap, the current study explores the integration of various industrial solid wastes into sealing applications as a strategy to promote resource recycling. Furthermore, it investigates the influence of waterglass on the performance of these additive-modified sealing materials and evaluates their carbonation resistance.

Waterglass was found to enhance the impermeability of BBA-modified samples; however, an opposite trend was observed in samples modified with WIFA and AAW. This contrast is attributed to the alkaline nature of waterglass, which can initially dissolve certain inherent minerals, such as boehmite in AAW. Similar mineral dissolution phenomena have been reported in the context of alkali-activated materials (Ling et al., 2024b; Provis, 2018). Nevertheless, due to the relatively low dosages of waterglass used in this study, the extent of mineral dissolution is presumed to be minimal. Consequently, the corresponding increase in permeability remains limited, with values not exceeding 6.34×10^{-10} m/s.

In terms of carbonation resistance, waterglass demonstrated a beneficial effect in WIFA-modified samples, as evidenced by a reduced degradation level of impermeability following carbonation exposure. Two primary mechanisms are proposed to account for this improvement. First, the increased alkalinity content enhances the CO_2 absorption capacity of the matrix, which can delay the diffusion of CO_2 into the sealing materials. Second, carbonation is inherently an acidification process, during which waterglass tends to hydrolyze and form silica gel. This is supported by the FT-IR analysis results presented in Fig. 7. The resulting silica gel may contribute to pore refinement and further impede CO_2 penetration.

To enhance the recycling of industrial wastes from diverse sources, this study utilized a variety of waste materials to prepare sealing materials for performance evaluation. In terms of impermeability, additives with finer particle size, such as AAW, yield the lowest permeability value of 4.04×10^{-12} m/s. This improvement is attributed to its filler effect, which enhances compacting density. Moreover, the content of alkaline-soluble components in the additives plays a critical role when waterglass is used to modify the impermeability. These soluble phases can initially undergo dissolution in the alkaline environment, potentially generating additional porosity that adversely affects the impermeability of the sealing matrix. With respect to carbonation resistance, variations in the chemical composition of the additives significantly influence the carbonation products. WIFA, characterized by high levels of leachable magnesium and calcium ions, promotes the formation of monohydrocalcite, magnesium carbonate, and calcite. In contrast, BBA, which primarily contains leachable calcium, predominantly results in calcite precipitation. AAW, with comparatively lower concentrations of leachable Mg and Ca, exhibits reduced CO_2 adsorption and limited carbonate formation, indicating weaker carbonation activity. From an environmental perspective, WIFA presents potential risks due to its high levels of leachable chloride and antimony, particularly after the diffusion of CO_2. However, it is worth noting that the landfill leachate is typically collected and treated to prevent environmental contamination. Therefore, no immediate environmental risk is posed by the sealing materials developed in this study. Nevertheless, industrial solid wastes with low levels of leachable toxic elements are still preferred, considering the additional costs and burdens associated with further leachate treatment. In summary, the selection of industrial solid wastes as additives in sealing materials should prioritize materials with fine particle sizes and low contents of leachable Mg, Ca, and environmentally hazardous elements.

5. Conclusions

The primary objective of this study is to assess the effects of carbonation on landfill sealing materials derived from various Dutch industrial by-products. DSS was used as the matrix material, while WIFA, BBA and AAW served as additives. The compacted layer materials were prepared as alternative landfill sealing materials for landfill cover systems and subjected to accelerated carbonation. The permeability, chemical and physical changes, and leaching behavior were comprehensively analyzed. Based on the results obtained, the following conclusions can be drawn:

1. Landfill sealing materials formulated with various solid wastes exhibit favorable impermeability properties ($< 6.34 \times 10^{-10}$ m/s), supporting their application as residual-based sealing layers in final landfill cover systems. Among these, the AAW-modified sealing material with 1.5 wt% waterglass achieves the lowest permeability (4.04×10^{-12} m/s), attributed to the finer particle size of AAW, which promotes pore refinement and matrix densification.

2. Carbonation process increases the permeability of sealing materials, accompanied by the formation of calcite, magnesium carbonate and monohydrocalcite. These carbonation products are associated with the availability of leachable Ca and Mg ions in the respective additives. The deterioration of impermeability is due to the development of capillary pores caused by volume changes between the original calcium-bearing phase and carbonation products.
3. Waterglass serves as a binder that improves matrix densification and impermeability. However, its high alkalinity can initially dissolve reactive mineral phases in the additives, increasing porosity and partially compromising impermeability. In contrast, waterglass enhances carbonation resistance by raising alkalinity to promote CO_2 absorption and forming silica gel to fill pores and limit CO_2 diffusion.
4. WIFA-modified samples exhibit high levels of leachable chloride and antimony, which can be attributed to the inherent characteristics of WIFA. Carbonation further increases the leachability of toxic elements. Since landfill leachate is systematically collected, the sealing materials developed in this study pose no immediate risks to the environment. However, when considering the additional costs and burdens associated with the leachate treatment, additives with low levels of leachable toxic elements, such as BBA and AAW, are recommended for use in the formulations of sealing materials.

This study focused on enhancing our comprehension of the impact of carbonation on sewage sludge-based landfill sealing materials, facilitating a deeper understanding of the factors influencing the longevity of these materials, particularly from the perspective of carbonation. The sewage sludge-based sealing materials are characterized by desirable impermeability and reduced environmental impact following carbonation, thus offering promising avenues for sustainable waste management practices. However, the accelerated carbonation process employed in this study still exhibits variations compared to the natural carbonation process, particularly in terms of CO_2 concentration, pressure, temperature, etc., suggesting room for further enhancement to provide more accurate results.

CRediT authorship contribution statement

H.J.H. Brouwers: Writing – review & editing, Project administration, Funding acquisition. **Katrin Schollbach:** Writing – review & editing, Investigation, Funding acquisition. **Yuxuan Chen:** Writing – review & editing, Methodology, Investigation, Formal analysis, Data curation, Conceptualization. **Xuan Ling:** Writing – original draft, Methodology, Investigation, Formal analysis, Data curation, Conceptualization.

Declaration of Competing Interest

The authors declare that they have no known competing financial interests or personal relationships that could have appeared to influence the work reported in this paper.

Acknowledgements

This research was carried out under project number T20014 in the framework of the Research Program of the Materials Innovation Institute (M2i) (www.m2i.nl), supported by the Dutch government and supported by the funding of the China Scholarship Council (No. 201906950015) and Eindhoven University of Technology. The authors would like to thank Euro Trust Management for supplying all raw materials and the Ingenieurbüro Kügler for the experimental tests. The support by and the discussions with Mr. J. Winter (ETM), Mr. H. Beukema (ETM) and Dr. J. Steketee (TAUW) are appreciated.

Appendix A. Supporting information

Supplementary data associated with this article can be found in the online version at doi:10.1016/j.psep.2025.107475.

References

Alba, N., Vázquez, E., Gassó, S., Baldasano, J.M., 2001. Stabilization/solidification of MSW incineration residues from facilities with different air pollution control systems: durability of matrices versus carbonation. Waste Manag. 21, 313–323. https://doi.org/10.1016/S0956-053X(00)00082-9.

Ayininuola, G.M., Ayodeji, I.O., 2016. Influence of sludge ash on soil shear strength. J. Civ. Eng. Res. 6, 72–77. https://doi.org/10.5923/j.jce.20160603.04.

Barlaz, M.A., Chanton, J.P., Green, R.B., 2009. Controls on landfill gas collection efficiency: instantaneous and lifetime performance. J. Air Waste Manag. Assoc. 59, 1399–1404. https://doi.org/10.3155/1047-3289.59.12.1399.

Bernal, S.A., Provis, J.L., Walkley, B., San Nicolas, R., Gehman, J.D., Brice, D.G., Kilcullen, A.R., Duxson, P., Van Deventer, J.S.J., 2013. Gel nanostructure in alkali-activated binders based on slag and fly ash, and effects of accelerated carbonation. Cem. Concr. Res. 53, 127–144. https://doi.org/10.1016/j.cemconres.2013.06.007.

Boels, D., Bril, J., Hummelink, E., Boersma, O., 2005. Wageningen. Durab. Hydrostab a Field Investig. Progn.

Böke, H., Akkurt, S., Özdemir, S., Göktürk, E.H., Caner Saltik, E.N., 2004. Quantification of CaCO3–CaSO3·0.5H2O–CaSO4·2H2O mixtures by FTIR analysis and its ANN model. Mater. Lett. 58, 723–726. https://doi.org/10.1016/j.matlet.2003.07.008.

Brunauer, S., Emmett, P.H., Teller, E., 1938. Adsorption of gases in multimolecular Layers. J. Am. Chem. Soc. 60, 309–319. https://doi.org/10.1021/ja01269a023.

Cheng, L., Chen, Y., Liu, T., Brouwers, H.J.H., Yu, Q., 2024. Understanding the CaCO3 phase transition of carbonated wollastonite composites caused by sodium tripolyphosphate: from amorphous to crystalline. Cem. Concr. Compos 148, 105477. https://doi.org/10.1016/j.cemconcomp.2024.105477.

Cheng, L., Chen, Y., Song, Z., Deng, Q., Yu, Q., 2025. Effects of relative humidity on carbonation kinetics and strength development of carbonated wollastonite composites containing sodium tripolyphosphate. Cem. Concr. Compos 155, 105831. https://doi.org/10.1016/j.cemconcomp.2024.105831.

Chukanov, N.V., 2014. Infrared spectra of mineral species. Extended library, 1st ed. Springer, Dordrecht.

Churio, M.S., Brusa, M.A., Grela, M.A., Bertolotti, S.G., Previtali, C.M., 2003. Time-resolved photoacoustic calorimetry of aqueous peroxodisulfate photolysis in the presence of nitrite anions. Phys. Chem. Chem. Phys. 5, 902–906. https://doi.org/10.1039/b209334k.

Council, E., 2002. Council Decision of 19 December 2002 establishing criteria and procedures for the acceptance of waste at landfills pursuant to article 16 of and Annex II to Directive 1999/31/EC. Off. J. Eur. Commun. 11, 27–49.

Duedall, I.W., 1972. The partial molal volume of calcium carbonate in sea water. Geochim. Cosmochim. Acta 36, 729–734. https://doi.org/10.1016/0016-7037(72)90083-X.

Dung, N.T., Hooper, T.J.N., Unluer, C., 2021. Improving the carbonation resistance of Na2CO3-activated slag mixes via the use of reactive MgO and nucleation seeding. Cem. Concr. Compos 115, 103832. https://doi.org/10.1016/j.cemconcomp.2020.103832.

Egloffstein, T.A., 2001. Natural bentonites—influence of the ion exchange and partial desiccation on permeability and self-healing capacity of bentonites used in GCLs. Geotext. Geomembr. 19, 427–444. https://doi.org/10.1016/S0266-1144(01)00017-6.

Gartung, E., Henken-Mellies, W.-U., Kanitz, J., Ramke, H.-G., 2010. Geotechnical aspects of landfill closure and aftercare. In: Chen, Y., Zhan, L., Tang, X. (Eds.), Advances in Environmental Geotechnics. Springer Berlin Heidelberg, Berlin, Heidelberg, pp. 188–203. https://doi.org/10.1007/978-3-642-04460-1_12.

Grénman, H., Salmi, T., Yu, D., Addai-mensah, J., 2010. Dissolution of boehmite in sodium hydroxide at ambient pressure: kinetics and modelling. Hydrometallurgy 102, 22–30. https://doi.org/10.1016/j.hydromet.2010.01.005.

Grootjes, A.J., Liakakou, E.T., Kuipers, H., Kooij, Y. van der, Wiermans, V., Zwart, R.W. R., 2019. Sludge to Power & Products (S2PP).

Gunning, P.J., Hills, C.D., Carey, P.J., 2010. Accelerated carbonation treatment of industrial wastes. Waste Manag. 30, 1081–1090. https://doi.org/10.1016/j.wasman.2010.01.005.

He, J., Li, F., Li, Y., Cui, X.L., 2015. Modified sewage sludge as temporary landfill cover material. Water Sci. Eng. 8, 257–262. https://doi.org/10.1016/j.wse.2015.03.003.

Herrmann, I., Andreas, L., Diener, S., Lind, L., 2010. Steel slag used in landfill cover liners: laboratory and field tests. Waste Manag. Res. 28, 1114–1121. https://doi.org/10.1177/0734242×10365095.

Herrmann, I., Svensson, M., Ecke, H., Kumpiene, J., Maurice, C., Andreas, L., Lagerkvist, A., 2009. Hydraulic conductivity of fly ash–sewage sludge mixes for use in landfill cover liners. Water Res. 43, 3541–3547. https://doi.org/10.1016/j.watres.2009.04.052.

Hua, M., Wang, B., Chen, L., Wang, Y., Quynh, V.M., He, B., Li, X., 2010. Verification of lime and water glass stabilized FGD gypsum as road sub-base. Fuel 89, 1812–1817. https://doi.org/10.1016/j.fuel.2009.11.029.

Huang, J., Chen, Y., Yu, Q., 2025. Amorphous calcium carbonate formation from carbonated recycled cement powder: a novel carbonation-activated cementitious material. Compos. Part B 297, 112336. https://doi.org/10.1016/j.compositesb.2025.112336.

Hyun, J., Kim, M.G., 2012. Field testing of conversion of sewage sludge to daily landfill cover material. J. Mater. Cycles Waste Manag. 14, 14–18. https://doi.org/10.1007/s10163-011-0034-9.
Iqbal, M.R., Hashimoto, K., Tachibana, S., Kawamoto, K., 2019. Geotechnical properties of sludge blended with crushed concrete and incineration ash. Int. J. Geomate 16, 116–123. https://doi.org/10.21660/2019.57.8130.
Jafari, N.H., Stark, T.D., Thalhamer, T., 2017. Progression of elevated temperatures in municipal solid waste landfills. J. Geotech. Geoenviron. Eng. 143, 05017004. https://doi.org/10.1061/(asce)gt.1943-5606.0001683.
Leemann, A., Moro, F., 2017. Carbonation of concrete: the role of CO2 concentration, relative humidity and CO2 buffer capacity. Mater. Struct. Constr. 50, 1–14. https://doi.org/10.1617/s11527-016-0917-2.
Li, N., Farzadnia, N., Shi, C., 2017. Microstructural changes in alkali-activated slag mortars induced by accelerated carbonation. Cem. Concr. Res. 100, 214–226. https://doi.org/10.1016/j.cemconres.2017.07.008.
Li, Y.L., Liu, J.W., Chen, J.Y., Shi, Y.F., Mao, W., Liu, H., Li, Y., He, S., Yang, J.K., 2014. Reuse of dewatered sewage sludge conditioned with skeleton builders as landfill cover material. Int. J. Environ. Sci. Technol. 11, 233–240. https://doi.org/10.1007/s13762-013-0199-y.
Li, B., Xiong, J., Peng, C., Li, M., Liu, H., Wang, W., Peng, S., 2023. Hierarchical porous AlOOH hollow microspheres for efficient CO2 capture. Ceram. Int. 49, 38226–38236. https://doi.org/10.1016/j.ceramint.2023.09.154.
Li, Z., Zhang, S., Zuo, Y., Chen, W., 2019. Chemical deformation of metakaolin based geopolymer. Cem. Concr. Res. 120, 108–118. https://doi.org/10.1016/j.cemconres.2019.03.017.
Lin, D., Lin, K., Hung, M., Luo, H., 2007. Sludge ash / hydrated lime on the geotechnical properties of soft soil, 145, 58–64. https://doi.org/10.1016/j.jhazmat.2006.10.087.
Ling, X., Chen, W., Schollbach, K., Brouwers, H.J.H., 2024a. Low permeability sealing materials based on sewage, digestate and incineration industrial by-products in the final landfill cover system. Constr. Build. Mater. 412, 134889. https://doi.org/10.1016/j.conbuildmat.2024.134889.
Ling, X., Chen, W., Schollbach, K., Brouwers, H.J.H., 2024b. Valorization of biomass bottom ash in alkali-activated GGBFS-fly ash: Impact of biomass bottom ash characteristic, silicate modulus and aluminum-anodizing waste. Constr. Build. Mater. 428, 136408. https://doi.org/10.1016/j.conbuildmat.2024.136408.
Ling, X., Schollbach, K., Chen, Y., Brouwers, H.J.H., 2024c. The effect of nano-silica and silica fume on the sodium carbonate-activated slag system containing air pollution control residues. Waste Manag 176, 52–63. https://doi.org/10.1016/j.wasman.2024.01.028.
Liu, G., Florea, M.V.A., Brouwers, H.J.H., 2021. The role of recycled waste glass incorporation on the carbonation behaviour of sodium carbonate activated slag mortar. J. Clean. Prod. 292, 126050. https://doi.org/10.1016/j.jclepro.2021.126050.
Liu, M., Lu, H., Deng, Q., Ji, S., Qin, L., Wan, Y., 2022. Shear strength, water permeability and microstructure of modified municipal sludge based on industrial solid waste containing calcium used as landfill cover materials. Waste Manag. 145, 20–28. https://doi.org/10.1016/j.wasman.2022.04.031.
Ma, Y., Hu, J., Ye, G., 2013. The pore structure and permeability of alkali activated fly ash. Fuel 104, 771–780. https://doi.org/10.1016/j.fuel.2012.05.034.
Morandeau, A., Thiéry, M., Dangla, P., 2015. Impact of accelerated carbonation on OPC cement paste blended with fly ash. Cem. Concr. Res. 67, 226–236. https://doi.org/10.1016/j.cemconres.2014.10.003.
Myers, R.J., Bernal, S.A., Provis, J.L., 2014. Cement and concrete research A thermodynamic model for C- (N-) A-S-H gel: CNASH _ ss. Derivation and validation. Cem. Concr. Res 66, 27–47. https://doi.org/10.1016/j.cemconres.2014.07.005.
Nishiyama, R., Munemoto, T., Fukushi, K., 2013. Formation condition of monohydrocalcite from CaCl2–MgCl2–Na2CO3 solutions. Geochim. Cosmochim. Acta 100, 217–231. https://doi.org/10.1016/j.gca.2012.09.002.
Olszak-Humienik, M., 2001. On the thermal stability of some ammonium salts. Thermochim. Acta 378, 107–112. https://doi.org/10.1016/S0040-6031(01)00585-8.
Paulik, F., Paulik, J., Arnold, M., 1992. Thermal decomposition of gypsum. Thermochim. Acta 200, 195–204. https://doi.org/10.1016/0040-6031(92)85115-C.
Provis, J.L., 2018. Alkali-activated materials. Cem. Concr. Res. 114, 40–48. https://doi.org/10.1016/j.cemconres.2017.02.009.
Rijkswaterstaat, 1991. Guidelines implementing the landfill decision on soil protection [WWW Document]. URL ⟨https://www.bodemplus.nl/@132149/richtlijnen-uitvoeringsregeling-stortbesluit/⟩.
Rijkswaterstaat Bodem+, 1991. Guidelines for the implementation of the landfill decree on soil protection.
Rodriguez-Navarro, C., Ruiz-Agudo, E., Luque, A., Rodriguez-Navarro, A.B., Ortega-Huertas, M., 2009. Thermal decomposition of calcite: mechanisms of formation and textural evolution of CaO nanocrystals. Am. Miner. 94, 578–593. https://doi.org/10.2138/am.2009.3021.
Rosli, N.A., Aziz, H.A., Selamat, M.R., Lim, L.L.P., 2020. A mixture of sewage sludge and red gypsum as an alternative material for temporary landfill cover. J. Environ. Manag. 263, 110420. https://doi.org/10.1016/J.JENVMAN.2020.110420.
Rubinos, D.A., Spagnoli, G., 2018. Utilization of waste products as alternative landfill liner and cover materials–A critical review. Crit. Rev. Environ. Sci. Technol. 48, 376–438. https://doi.org/10.1080/10643389.2018.1461495.
Sabrin, S., Nazari, R., Fahad, M.G.R., Karimi, M., Everett, J.W., Peters, R.W., 2020. Investigating effects of landfill soil gases on landfill elevated subsurface temperature. Appl. Sci. 10. https://doi.org/10.3390/APP10186401.
Sadasivam, B.Y., Reddy, K.R., 2015. Adsorption and transport of methane in landfill cover soil amended with waste-wood biochars. J. Environ. Manag. 158, 11–23. https://doi.org/10.1016/j.jenvman.2015.04.032.
Sanchez, F., Gervais, C., Garrabrants, A.C., Barna, R., Kosson, D.S., 2002. Leaching of inorganic contaminants from cement-based waste materials as a result of carbonation during intermittent wetting. Waste Manag. 22, 249–260. https://doi.org/10.1016/S0956-053X(01)00076-9.
Scrivener, K., Snellings, R., Lothenbach, B., 2016. A practical guide to microstructural analysis of cementitious materials. Crc Press, Boca Raton, FL, USA.
Serafeimidis, K., Anagnostou, G., 2014. On the crystallisation pressure of gypsum. Environ. Earth Sci. 72, 4985–4994. https://doi.org/10.1007/s12665-014-3366-7.
Shafique, M.S.Bin, Walton, J.C., Gutierrez, N., Smith, R.W., Tarquin, A.J., 1998. Influence of carbonation on leaching of cementitious wasteforms. J. Environ. Eng. 124, 463–467. https://doi.org/10.1061/(ASCE)0733-9372(1998)124:5(463).
Shi, Z., Shi, C., Wan, S., Li, N., Zhang, Z., 2018. Effect of alkali dosage and silicate modulus on carbonation of alkali-activated slag mortars. Cem. Concr. Res. 113, 55–64. https://doi.org/10.1016/j.cemconres.2018.07.005.
Sing, K.S.W., 1985. Reporting physisorption data for gas/solid systems with special reference to the determination of surface area and porosity (Recommendations 1984). Pure Appl. Chem. Pure Appl. Chem. 57, 603–619. https://doi.org/10.1351/pac198557040603.
Singman, C.N., 1984. Atomic volume and allotropy of the elements. J. Chem. Educ. 61, 137. https://doi.org/10.1021/ed061p137.
Song, K.-I., Song, J.-K., Lee, B.Y., Yang, K.-H., 2014. Carbonation characteristics of alkali-activated blast-furnace slag mortar. Adv. Mater. Sci. Eng. 2014, 326458. https://doi.org/10.1155/2014/326458.
Spokas, K., Bogner, J., Chanton, J.P., Morcet, M., Aran, C., Graff, C., Golvan, Y.M.-L., Hebe, I., 2006. Methane mass balance at three landfill sites: what is the efficiency of capture by gas collection systems. Waste Manag. 26, 516–525. https://doi.org/10.1016/j.wasman.2005.07.021.
Taki, K., Choudhary, S., Gupta, S., Kumar, M., 2020. Enhancement of geotechnical properties of municipal sewage sludge for sustainable utilization as engineering construction material. J. Clean. Prod. 251, 119723. https://doi.org/10.1016/J.JCLEPRO.2019.119723.
Tramontin, M., Simão, L., Rubem, O., Montedo, K., Raupp, F., Pedro, A., Oliveira, N., De, 2019. Aluminum anodizing waste and its uses: an overview of potential applications and market opportunities. Waste Manag. 84, 286–301. https://doi.org/10.1016/j.wasman.2018.12.003.
Turnbull, A.G., 1973. A thermochemical study of monohydrocalcite. Geochim. Cosmochim. Acta 37, 1593–1601. https://doi.org/10.1016/0016-7037(73)90093-8.
Valls, S., Vàzquez, E., 2001. Accelerated carbonatation of sewage sludge-cement-sand mortars and its environmental impact. Cem. Concr. Res. 31, 1271–1276. https://doi.org/10.1016/S0008-8846(01)00573-7.
Wagner, J.F., 2013. Clay Liners and Waste Disposal. Developments in Clay Science, 2nd ed. Elsevier Ltd. https://doi.org/10.1016/B978-0-08-098259-5.00023-8.
Wang, S.Y., McCaslin, E., White, C.E., 2020. Effects of magnesium content and carbonation on the multiscale pore structure of alkali-activated slags. Cem. Concr. Res. 130, 105979. https://doi.org/10.1016/j.cemconres.2020.105979.
Wiśniewska, M., Stępniewski, W., 2006. The influence of lime, water-glass and clay addition on sealing properties of waste rock from Bogdanka. September 2005. In: Environmental Engineering: Proceedings of the 2nd National Congress on Environmental Engineering, 4-8. CRC Press, p. 271. September 2005.
Yao, Q., Zhou, G., 2015. Transformation of amorphous calcium carbonate into Monohydrocalcite in aqueous solution: A biomimetic mineralization study. Transform. Amorph. Calcium Carbonate Into Monohydrocalcite Aqueous Solut. a Biomim. Miner. Study. https://doi.org/10.1127/ejm/2015/0027-2486.
Zhang, Z., Scherer, G.W., 2019. Evaluation of drying methods by nitrogen adsorption. Cem. Concr. Res. 120, 13–26. https://doi.org/10.1016/j.cemconres.2019.02.016.